Electronic supplementary material

Simultaneous removal of heavy metal ions by sulfonic acid-functionalized melamine-based covalent organic framework: Optimization by surface response methodology

Asiyeh Salami [a], Arash Larki [a]*, Seyyed Jafar Saghanezhad [b]

[a] *Department of Marine Chemistry, Faculty of Marine Science, Khorramshahr University of Marine Science and Technology, Khorramshahr, Iran*
[b] *ACECR-Production Technology Research Institute, Ahvaz, Iran*

***Corresponding author:**

Arash Larki, E-mail: arash_larki@yahoo.com & a.larki@kmsu.ac.ir

Contents:

S1. Adsorption study

Adsorption isotherms

In the Langmuir model, it is assumed that the adsorption is monolayer and occurs at a homogeneous surface, without interaction between the absorbed materials [1]. The linearity of the Langmuir model is described by the equation (1) as follows:

$$\frac{C_e}{q_e} = \frac{1}{K_L q_{max}} + \frac{C_e}{q_{max}} \quad (1)$$

where, C_e (mg L^{-1}) and q_e (mg g^{-1}) are heavy metal ions concentration and quantity of desired ions adsorbed onto the absorbent surface at equilibrium, q_{max} (mg g^{-1}) is the maximum adsorption capacity and K_L (mL mg^{-1}) is the Langmuir adsorption equilibrium constant. q_{max} and K_L could be calculated with a straight line drawn from of C_e/q_e versus C_e.

The Freundlich isotherm is not accept the capacity of one layer and is based on the assumption of adsorption on heterogeneous surfaces, due to the increase in the amount of analyte adsorbed in the solution [2]. This model is linear by the equation (2) as follows:

$$\log q_e = \log k_f + \left(\frac{1}{n}\right) \log C_e \quad (2)$$

where, n and K_F (mg g^{-1} (L $mg^{-1})^{1/n}$) are Freundlich constants, which are related to the heterogeneity factor and adsorption capacity, respectively. These constants can be calculated by plotting of $log\ q_e$ versus $log\ C_e$. The n value should be in the range 1 to 10 for favorable adsorption process.

The Temkin isotherm model contains a parameter which considers the adsorbent-adsorbate interactions and assumes that the adsorption heat declines linearly with the surface covered between the adsorbates and adsorbent [3]. The linearity of Temkin model is given by equation (3):

$$q_e = B\ln K_T + \left(\frac{RT}{b}\right)\ln C_e \quad (3)$$

where, $B=RT/b_T$, b_T (J mol^{-1}) is the constant of Temkin that is related to the heat of adsorption, K_T (L g^{-1}) is the equilibrium binding constant, R and T are the gas constant (8.3145 J mol^{-1} K^{-1}) and absolute temperature in Kelvin, respectively. The B and K_T values can be calculated from slope and intercept of a graph between q_e and lnC_e.

The Dubinin-Radushkevich (D-R) model isotherm can be distinguished between physical and chemical adsorption of metal ions. The D-R model is often used to estimate the characteristic porosity and the apparent free energy of adsorption [4]. The Dubinin-Radushkevich adsorption isotherm is represented as equation (4):

$$Ln\ q_e = ln\ q_m - \beta\ \varepsilon^2 \quad (4)$$

where β (mol^2/kJ^2) is a constant related to the mean free energy change, ε is the polanyi potential and could be determined by equation (5). The mean free energy (kJ mol^{-1}) could be calculated using equation (6):

$$\varepsilon = RT\ ln\left(1 + \frac{1}{C_e}\right) \quad (5)$$

$$E = \frac{1}{\sqrt{2\beta}}) \quad (6)$$

The Kahn isotherm model is a general model for adsorption of adsorbate from pure dilute equations solutions. This model has been used to describe the experimental data with the minimum average percentage error for the adsorption of some pollutants from aqueous solutions by comparing several multicomponent adsorption isotherms [5]. This isotherm model is expressed as equation (7):

$$q_e = \frac{q_m b_k C_e}{(1 + b_k C_e)^{ax}} \quad (7)$$

where b_K is the Khan isotherm constant (L mg^{-1}) and a_K is the Khan isotherm model exponent.

The Langmuir isotherm diagram for Cd(II), Cu(II), Pb(II), Ni(II) and Zn(II) ions by COF@SO_3H (at 25 °C with pH of 5.5) is shown in Fig. S5 to S9, respectively.

Adsorption kinetics

The pseudo-first-order model was shown in equation (8):

$$ln\left(q_e - q_t\right) = ln\, q_e - K_1 t \tag{8}$$

where q_e and q_t (mg g^{-1}) were the amount of adsorbed ions at equilibrium and at time t; k_1 (min^{-1}) was the rate constant of the pseudo-first-order model. Through drawing the plot of $ln(q_e\text{-}q_t)$ vs. t, q_e and k_1 were calculated as the slope and intercept.

In addition, equation (9) gave a model of the pseudo-second-order:

$$\frac{t}{q_t} = \frac{1}{k_2 q_e^2} + \frac{1}{q_e} \tag{9}$$

where, k_2 (g mg^{-1} min^{-1}) was the rate constant of pseudo-second-order adsorption [6, 7]. From the slope and intercept of the plots t/q_t vs. t, the pseudo-second-order rate constant k_2 and q_e values were acquired.

To identify the diffusion mechanism in the adsorption, intraparticle mass transfer diffusion model has been proposed by Weber and Morris [8]. The equation (10) may be written as follows:

$$q_t = K_{dif} t^{1/2} + C \tag{10}$$

where k_{dif} is the intraparticle diffusion constant (g g^{-1} $min^{-1/2}$) and C (g g^{-1}) a constant related with diffusion resistance.

The Kinetic model for Cd(II), Cu(II), Pb(II), Ni(II) and Zn(II) ions adsorption onto the COF@SO_3H adsorbent using pseudo-2nd-order are shown in Fig. S10 to S14, respectively.

Table S1. Experimental results of adsorption tests in removal of target ions under BBD.

	Factor 1	Factor 2	Factor 3	Factor 4	Response 1	Response 2	Response 3	Response 4	Response 5
Run	A pH	B Ads. Dos. (mg)	C Inicial Conc. (mg/L)	D time (min)	Cd Removal (%)	Pb Removal (%)	Cu Removal (%)	Zn Removal (%)	Ni Removal (%)
1	7	25	3	20	64	58	66.9	66	68
2	7	25	1	40	63.9	62	65	63.1	63.7
3	5.5	10	1	40	79.5	78	80.3	80.1	79.6
4	4	25	1	40	97.3	98.1	95.9	99.6	98
5	5.5	10	3	60	65.9	68	64	66	65.7
6	7	25	3	60	60.4	60.7	68.1	62.7	63.2
7	5.5	25	5	60	92	90.29	90.88	92.6	91.9
8	5.5	25	3	40	96.6	96.1	90.6	98.4	97.5
9	5.5	40	5	40	91.44	92.06	92.17	93	92.5
10	5.5	40	3	20	86.2	80.7	84.5	80.4	80
11	5.5	40	1	40	99.7	99.8	98.3	98	97.9
12	5.5	10	3	20	59.9	58.5	56.8	56.6	56.7
13	5.5	25	3	40	97.8	94.3	89	95	98
14	5.5	25	1	20	94.9	95.1	94.3	94	93.9
15	7	40	3	40	59.8	58	66.2	64	65
16	5.5	40	3	60	99.5	99.8	98.3	98	97.6
17	4	10	3	40	50.24	49.3	49	51	52.5
18	5.5	25	5	20	76.4	75.3	75.9	77.6	77
19	7	10	3	40	35.3	34	34.5	37	33
20	5.5	25	3	40	94.4	92.3	88	92.5	93.3
21	5.5	10	5	40	45.1	47.6	44.8	45.8	45
22	5.5	25	1	60	99.9	99.9	99.9	98.9	98.5
23	4	25	5	40	60.2	58.5	59.9	60.5	60
24	5.5	25	3	40	94	92.9	91	97.5	97.1
25	5.5	25	3	40	93.5	90.7	87	92	94.2
26	4	40	3	40	86.7	80	85.3	81.7	82
27	4	25	3	20	70.3	69.9	71.5	69.4	70
28	7	25	5	40	55.2	47.9	56.1	59	62.1
29	4	25	3	60	88	86	85	87.5	81

Table S2. ANOVA results for Cd(II) ion removal.

Source	Sum of Squares	df	Mean Square	F-value	p-value	
Model	10084.98	10	1008.50	93.07	< 0.0001	significant
A-pH	1085.66	1	1085.66	100.19	< 0.0001	
B-Ads. Dos.	2926.56	1	2926.56	270.08	< 0.0001	
C-Inicial Conc.	1099.40	1	1099.40	101.46	< 0.0001	
D-time	243.00	1	243.00	22.43	0.0002	
AB	35.76	1	35.76	3.30	0.0860	
AC	201.64	1	201.64	18.61	0.0004	
AD	113.42	1	113.42	10.47	0.0046	
BC	170.82	1	170.82	15.76	0.0009	
A^2	3406.98	1	3406.98	314.42	< 0.0001	
B^2	1300.19	1	1300.19	119.99	< 0.0001	
Residual	195.05	18	10.84			
Lack of Fit	181.37	14	12.96	3.79	0.1037	not significant
Pure Error	13.67	4	3.42			
Cor Total	10280.02	28				

Table S3. ANOVA results for Cu(II) ion removal.

Source	Sum of Squares	df	Mean Square	F-value	p-value	
Model	8685.45	9	965.05	103.14	< 0.0001	significant
A-pH	672.00	1	672.00	71.82	< 0.0001	
B-Ads. Dos.	3180.79	1	3180.79	339.96	< 0.0001	
C-Inicial Conc.	1082.05	1	1082.05	115.65	< 0.0001	
D-time	263.95	1	263.95	28.21	< 0.0001	
AC	183.60	1	183.60	19.62	0.0003	
AD	37.82	1	37.82	4.04	0.0588	
BC	215.65	1	215.65	23.05	0.0001	
A^2	2387.66	1	2387.66	255.19	< 0.0001	
B^2	1036.27	1	1036.27	110.76	< 0.0001	
Residual	177.77	19	9.36			
Lack of Fit	166.28	15	11.09	3.86	0.1004	not significant
Pure Error	11.49	4	2.87			
Cor Total	8863.22	28				

Table S4. ANOVA results for Pb(II) ion removal.

Source	Sum of Squares	df	Mean Square	F-value	p-value	
Model	10276.96	9	1141.88	85.78	< 0.0001	significant
A-pH	1224.12	1	1224.12	91.96	< 0.0001	
B-Ads. Dos.	2550.92	1	2550.92	191.62	< 0.0001	
C-Inicial Conc.	1225.13	1	1225.13	92.03	< 0.0001	
D-time	376.21	1	376.21	28.26	< 0.0001	
AC	162.56	1	162.56	12.21	0.0024	
AD	44.89	1	44.89	3.37	0.0820	
BC	128.37	1	128.37	9.64	0.0058	
A^2	3862.72	1	3862.72	290.17	< 0.0001	
B^2	1209.36	1	1209.36	90.85	< 0.0001	
Residual	252.93	19	13.31			
Lack of Fit	236.18	15	15.75	3.76	0.1048	not significant
Pure Error	16.75	4	4.19			
Cor Total	10529.89	28				

Table S5. ANOVA results for Ni(II) removal.

Source	Sum of Squares	df	Mean Square	F-value	p-value	
Model	8982.62	10	898.26	63.32	< 0.0001	significant
A-pH	652.69	1	652.69	46.01	< 0.0001	
B-Ads. Dos.	2369.50	1	2369.50	167.03	< 0.0001	
C-Inicial Conc.	885.80	1	885.80	62.44	< 0.0001	
D-time	174.47	1	174.47	12.30	0.0027	
AC	331.24	1	331.24	23.35	0.0002	
AD	62.41	1	62.41	4.40	0.0512	
BC	213.16	1	213.16	15.03	0.0012	
A^2	3117.98	1	3117.98	219.79	< 0.0001	
B^2	1591.20	1	1591.20	112.16	< 0.0001	
D^2	99.52	1	99.52	7.01	0.0169	
Residual	241.17	17	14.19			
Lack of Fit	223.18	13	17.17	3.82	0.1029	not significant
Pure Error	17.99	4	4.50			
Cor Total	9223.79	27				

Table S6. ANOVA results for Zn(II) ion removal.

Source	Sum of Squares	df	Mean Square	F-value	p-value	
Model	9367.92	10	936.79	76.28	< 0.0001	significant
A-pH	798.70	1	798.70	65.03	< 0.0001	
B-Ads. Dos.	2658.16	1	2658.16	216.43	< 0.0001	
C-Inicial Conc.	922.25	1	922.25	75.09	< 0.0001	
D-time	317.24	1	317.24	25.83	< 0.0001	
AC	306.25	1	306.25	24.94	< 0.0001	
AD	114.49	1	114.49	9.32	0.0068	
BC	214.62	1	214.62	17.47	0.0006	
A^2	3061.49	1	3061.49	249.27	< 0.0001	
B^2	1527.85	1	1527.85	124.40	< 0.0001	
D^2	53.03	1	53.03	4.32	0.0523	
Residual	221.07	18	12.28			
Lack of Fit	188.04	14	13.43	1.63	0.3409	not significant
Pure Error	33.03	4	8.26			
Cor Total	9588.99	28				

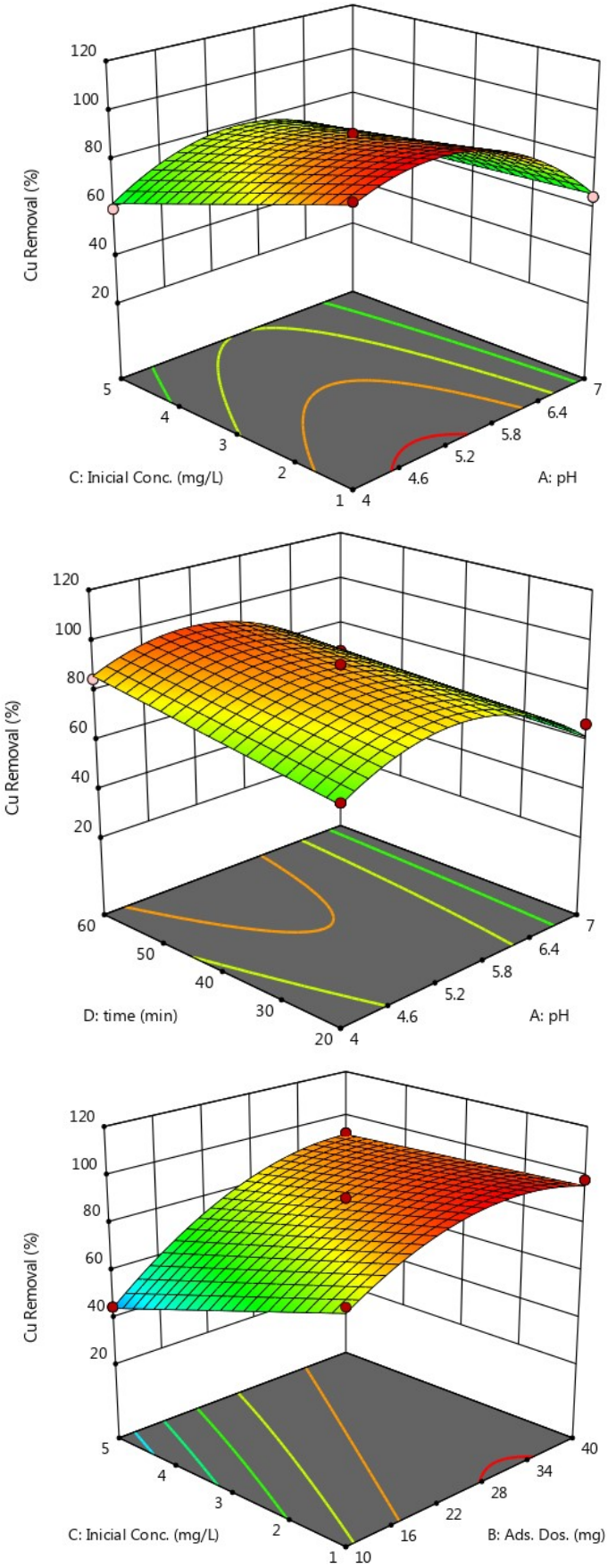

Fig. S1. 3D response surface plots of Cu(II) adsorption on COF@SO_3H adsorbent.

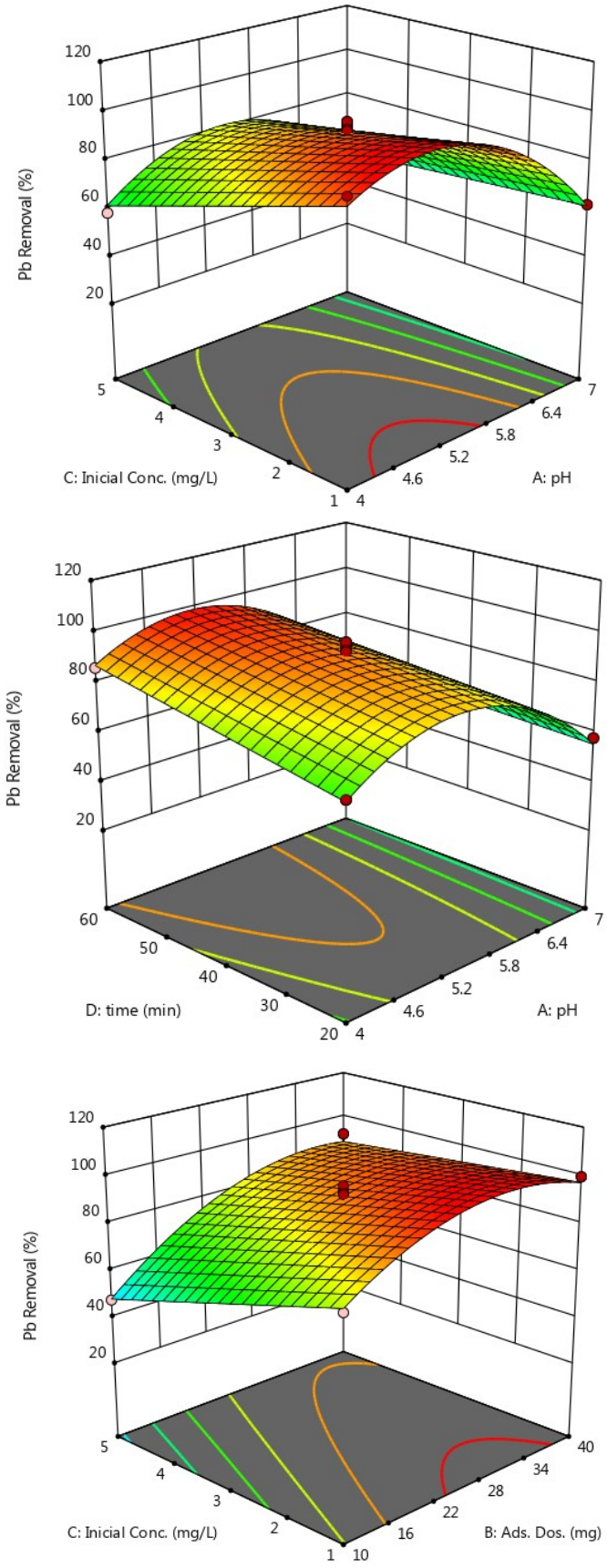

Fig. S2. 3D response surface plots of Pb(II) adsorption on COF@SO_3H adsorbent.

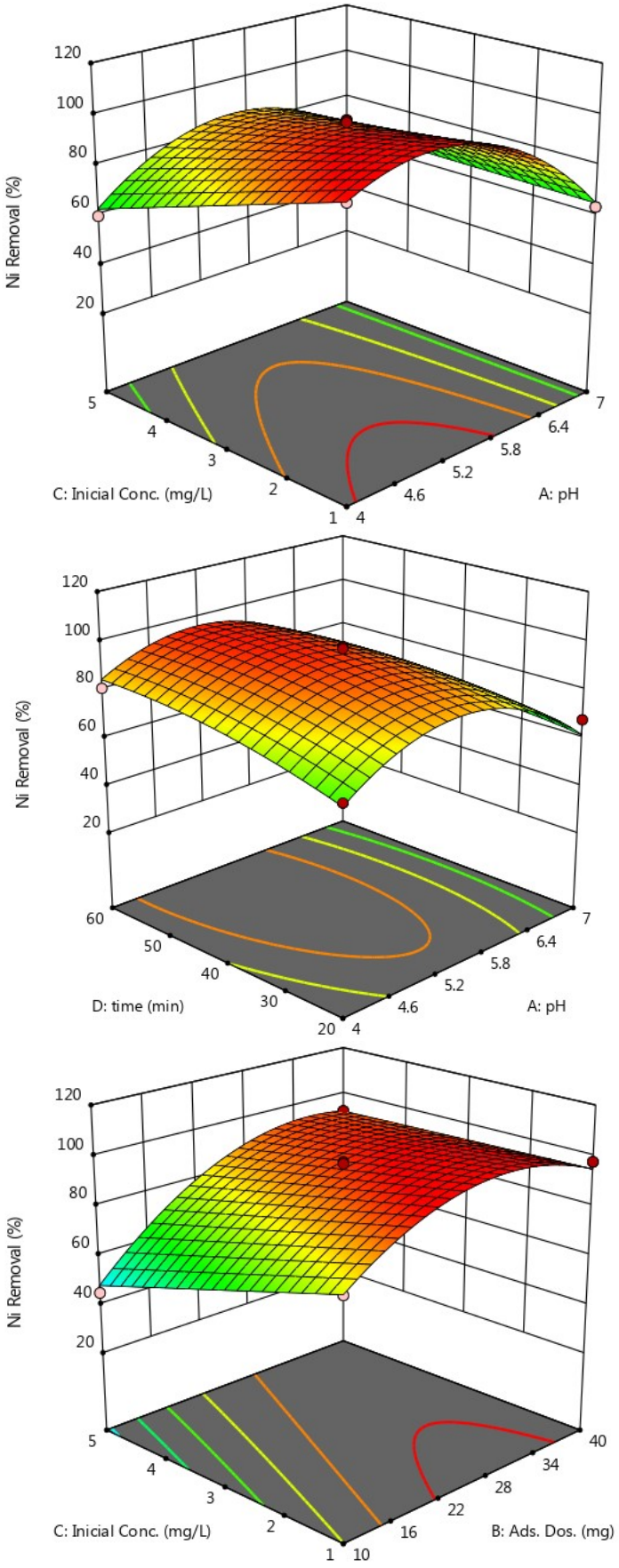

Fig. S3. 3D response surface plots of Ni(II) adsorption on COF@SO_3H adsorbent.

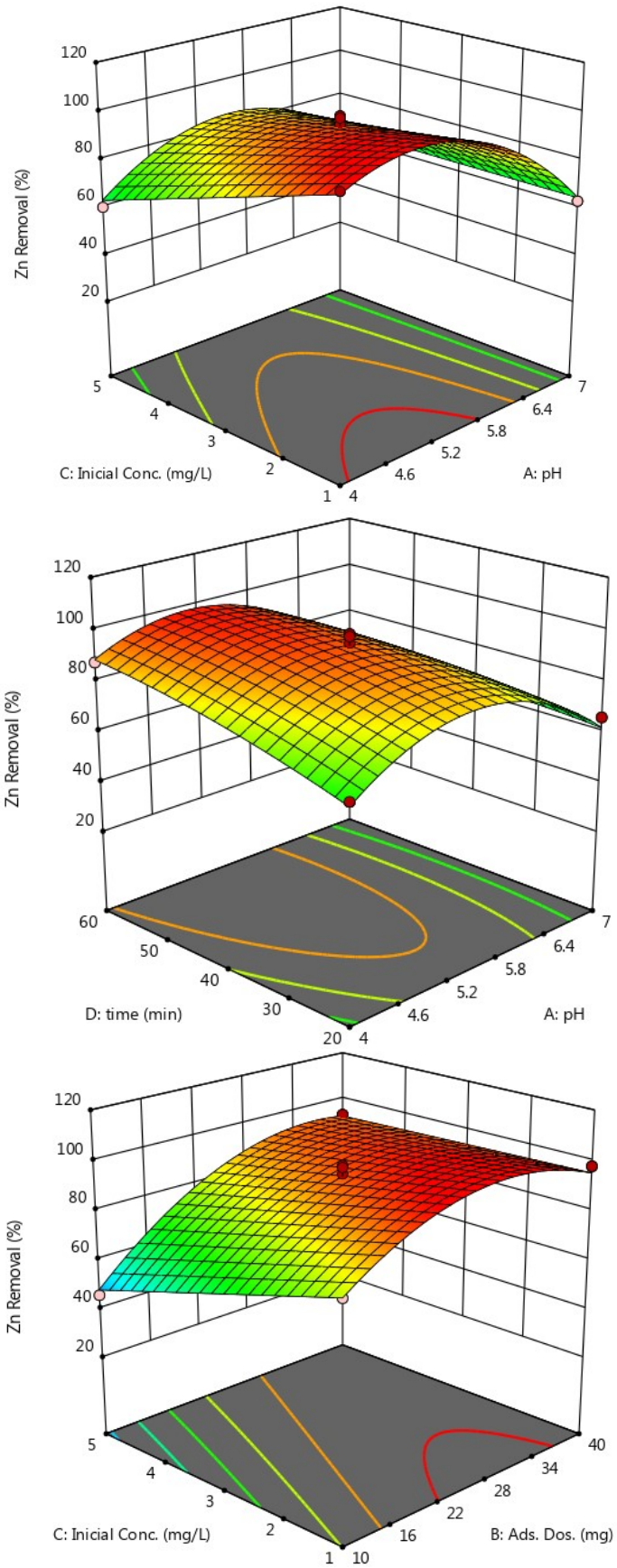

Fig. S4. 3D response surface plots of Zn(II) adsorption on COF@SO_3H adsorbent.

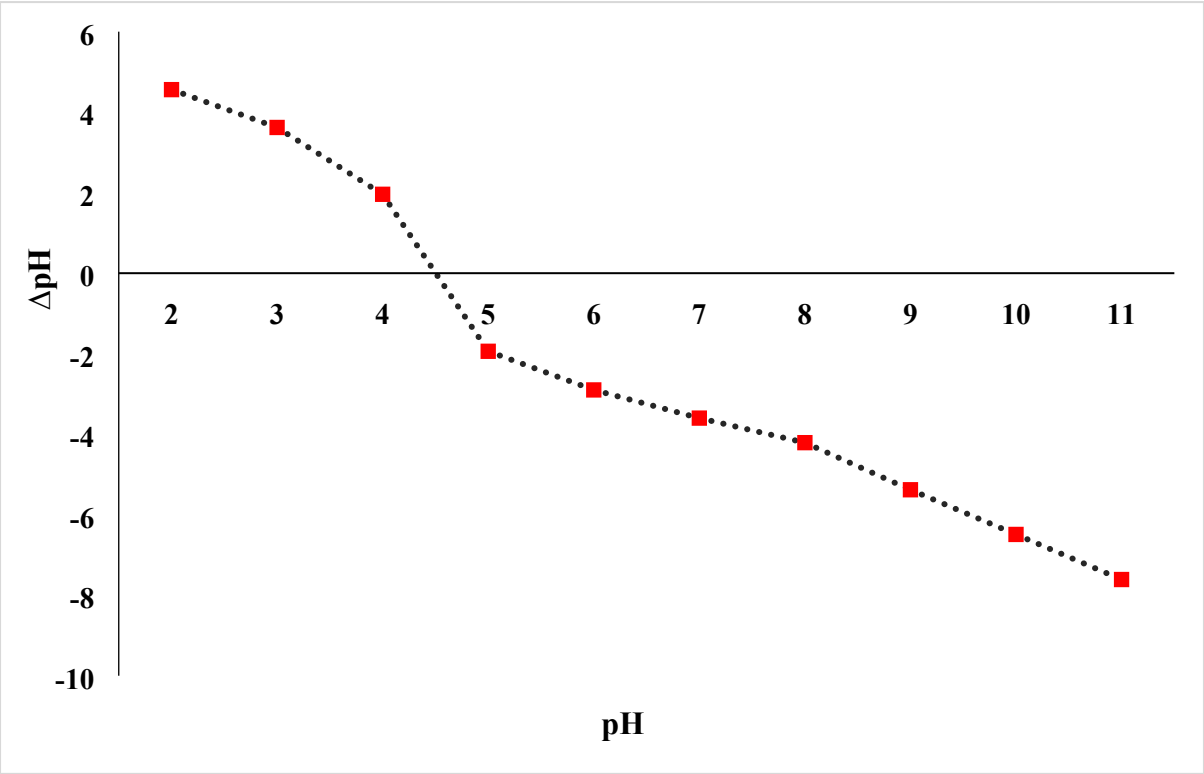

Fig. S5. Point Zero Charge (pHpzc) for COF@SO_3H adsorbent.

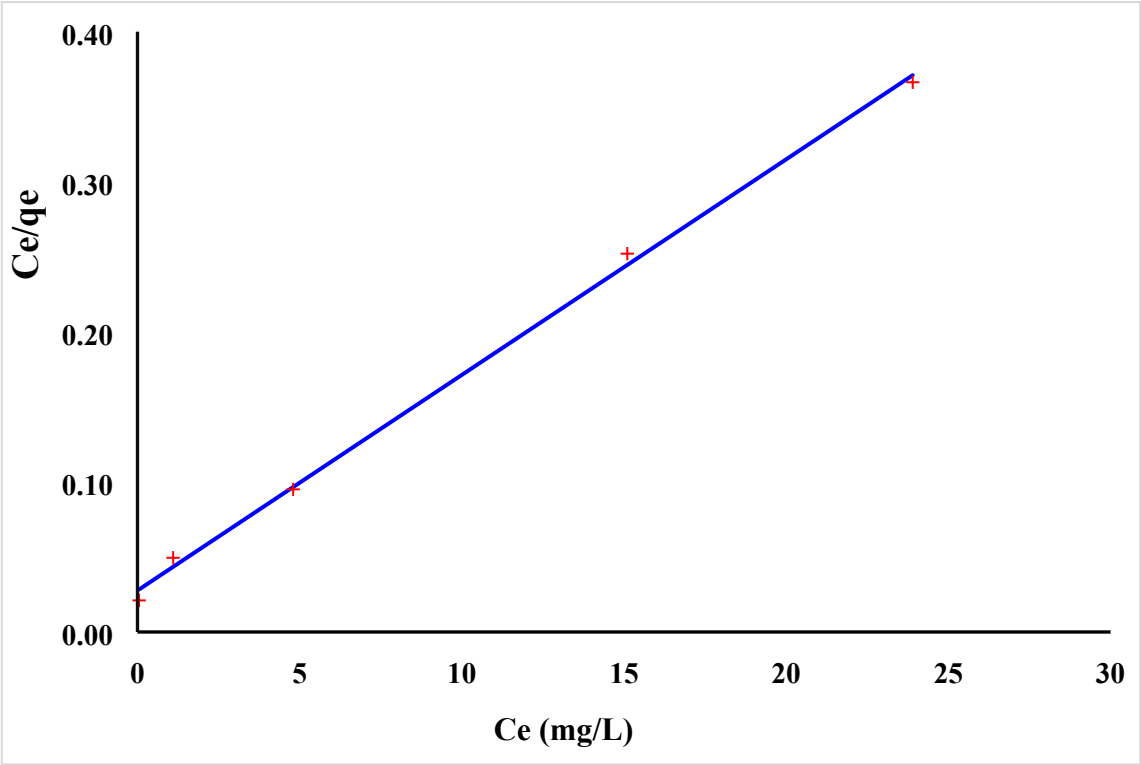

Fig. S6. Langmuir isotherm plot for Cd(II) removal by COF@SO_3H at 25 °C with pH of 5.5.

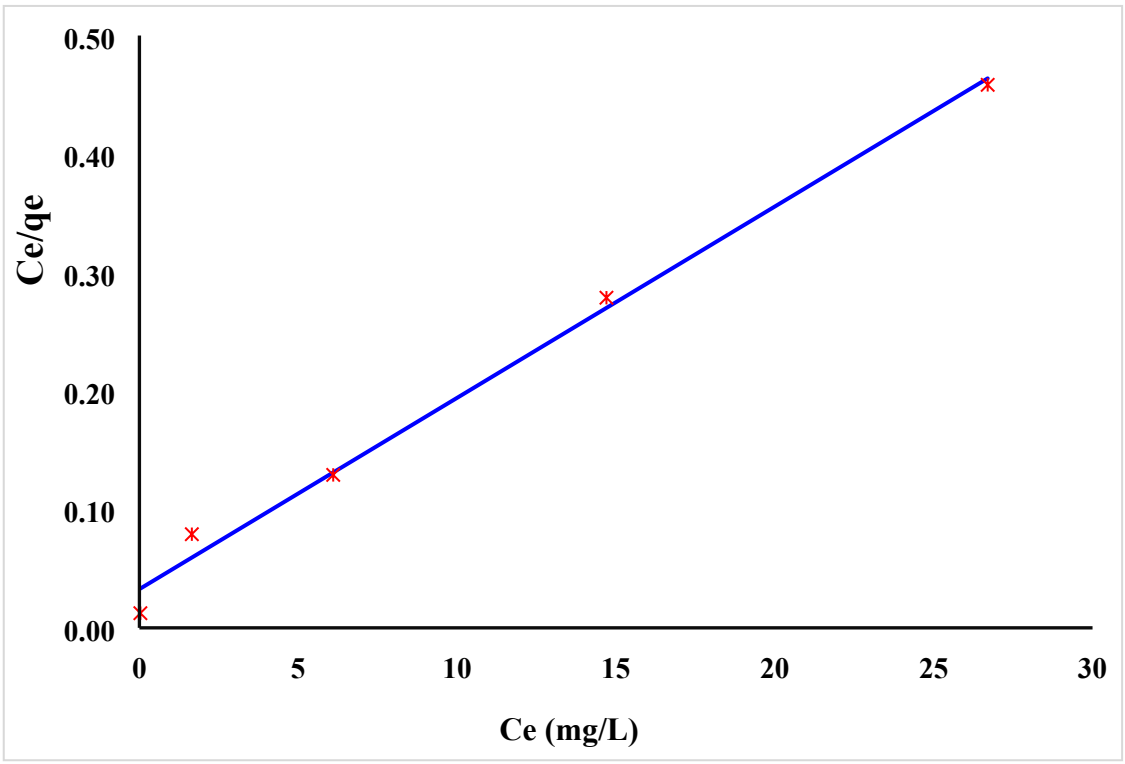

Fig. S7. Langmuir isotherm plot for Cu(II) removal by COF@SO_3H at 25 °C with pH of 5.5.

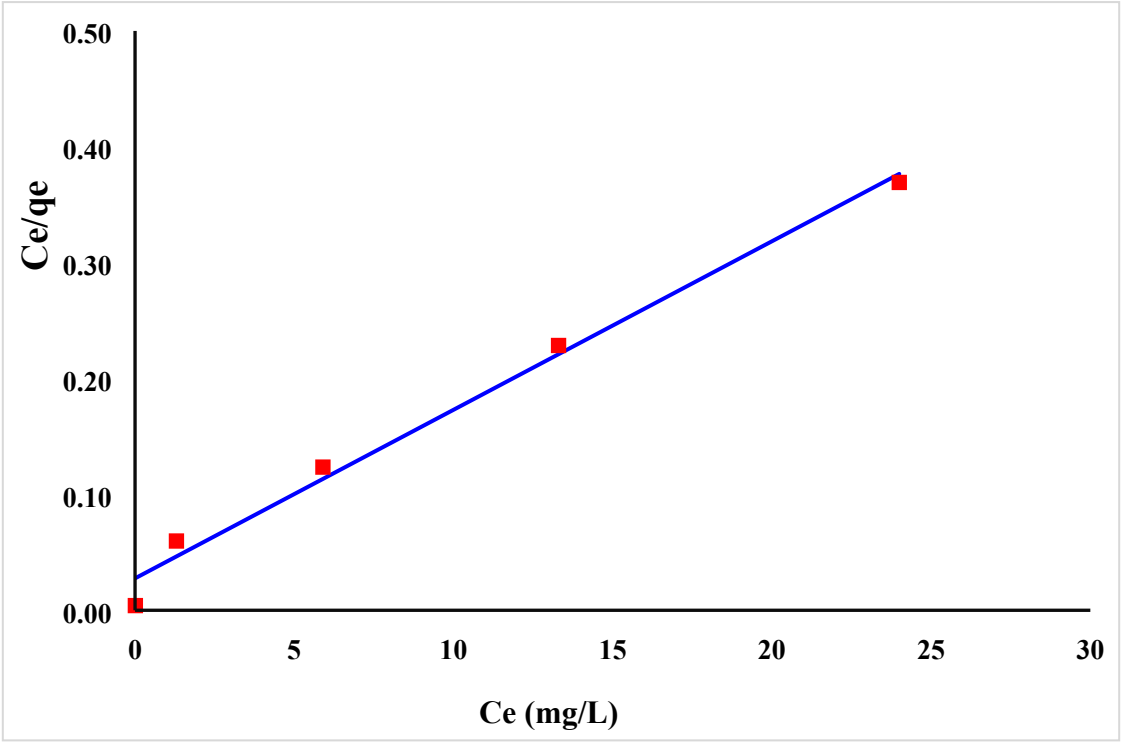

Fig. S8. Langmuir isotherm plot for Pb(II) removal by COF@SO_3H at 25 °C with pH of 5.5.

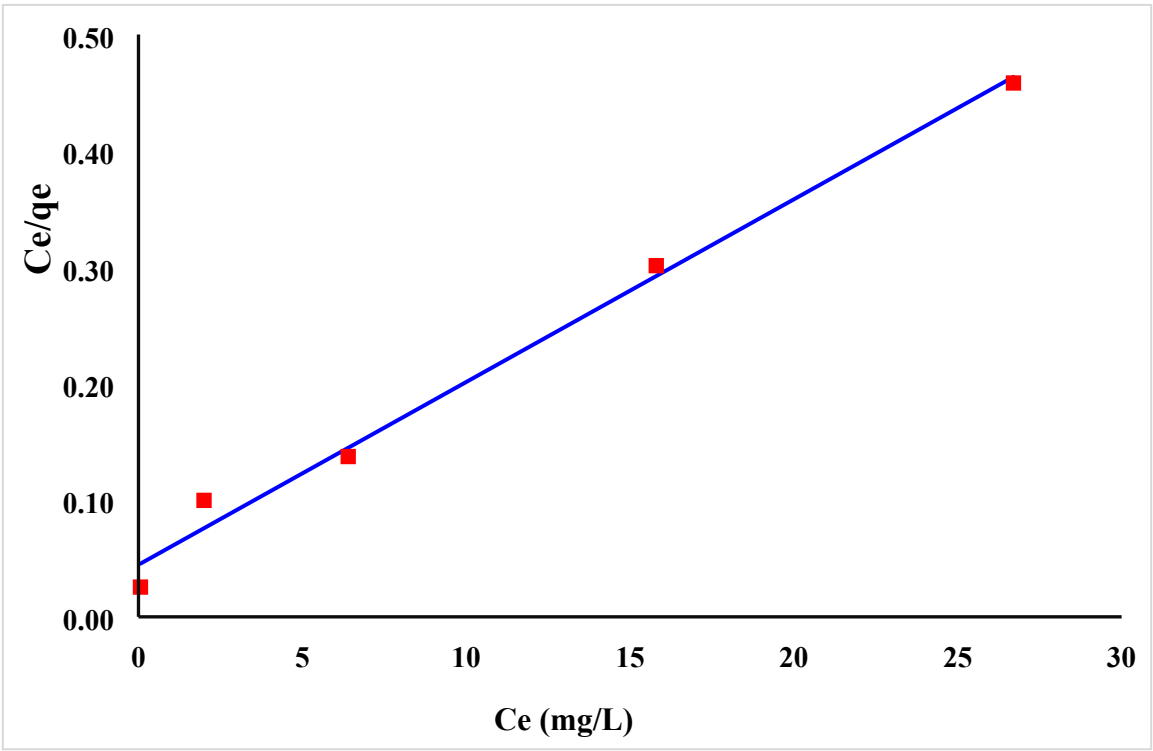

Fig. S9. Langmuir isotherm plot for Ni(II) removal by COF@SO_3H at 25 °C with pH of 5.5.

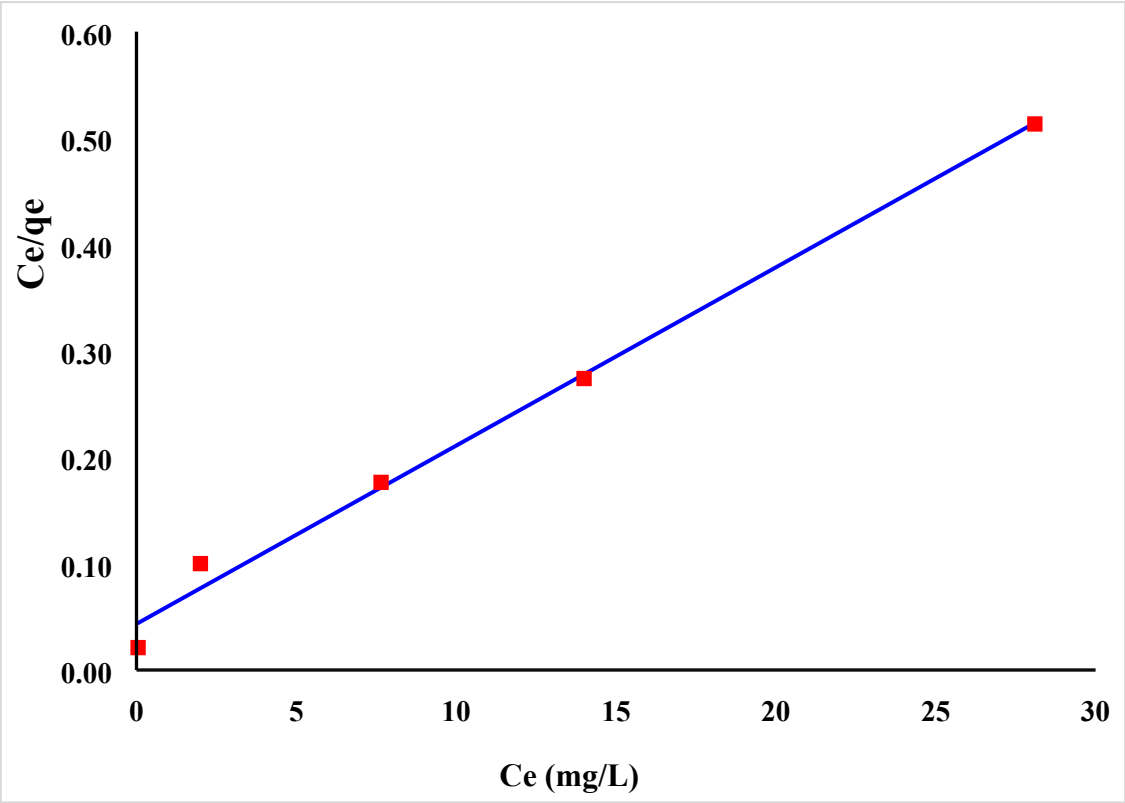

Fig. S10. Langmuir isotherm plot for Zn(II) removal by COF@SO_3H at 25 °C with pH of 5.5.

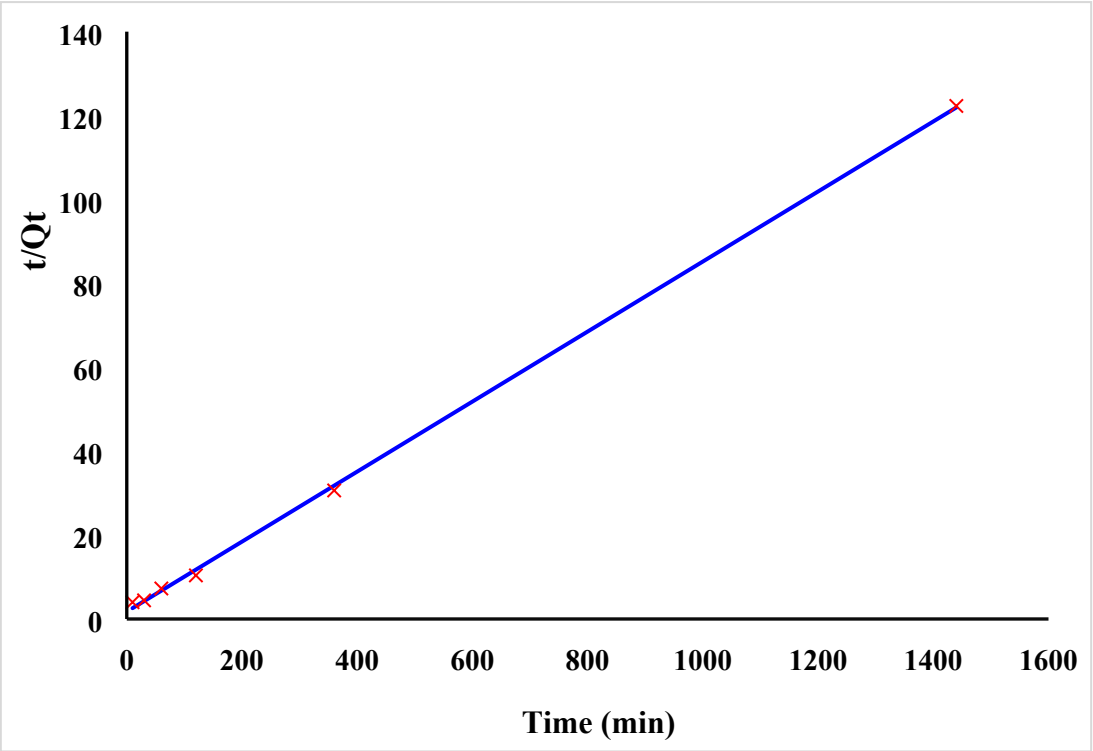

Fig. S11. Kinetic model of Cd(II) ions adsorption onto the COF@SO_3H adsorbent using pseudo-2nd-order.

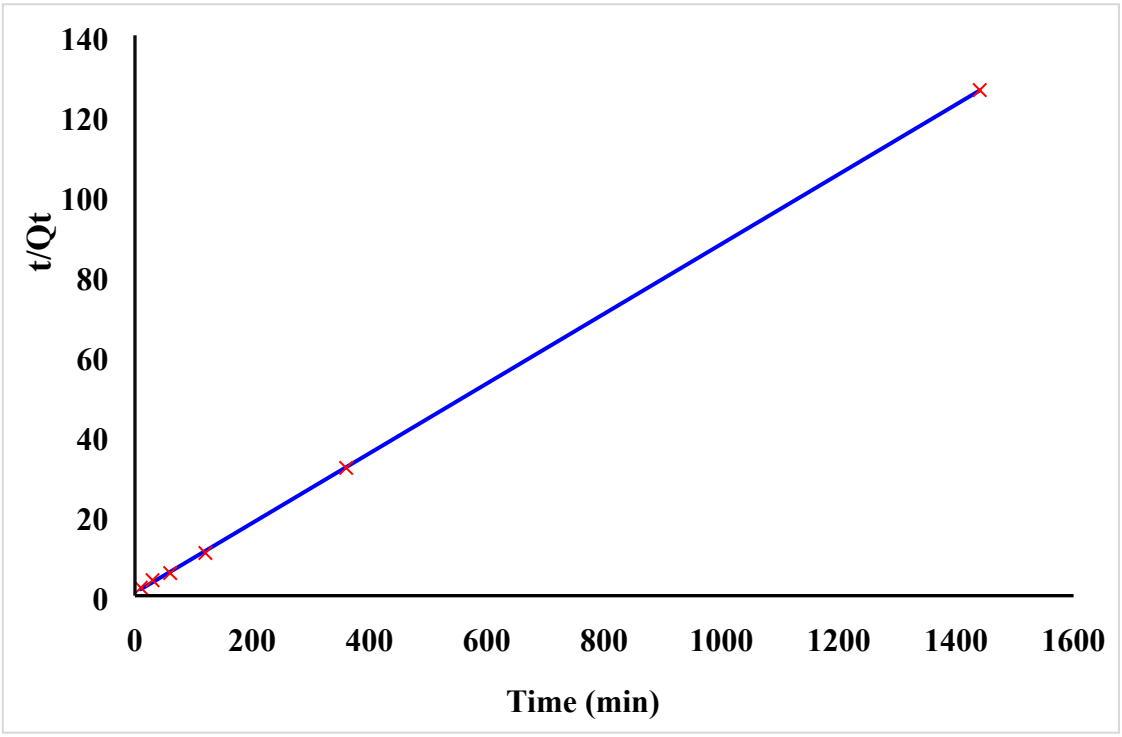

Fig. S12. Kinetic model of Cu(II) ions adsorption onto the COF@SO_3H adsorbent using pseudo-2nd-order.

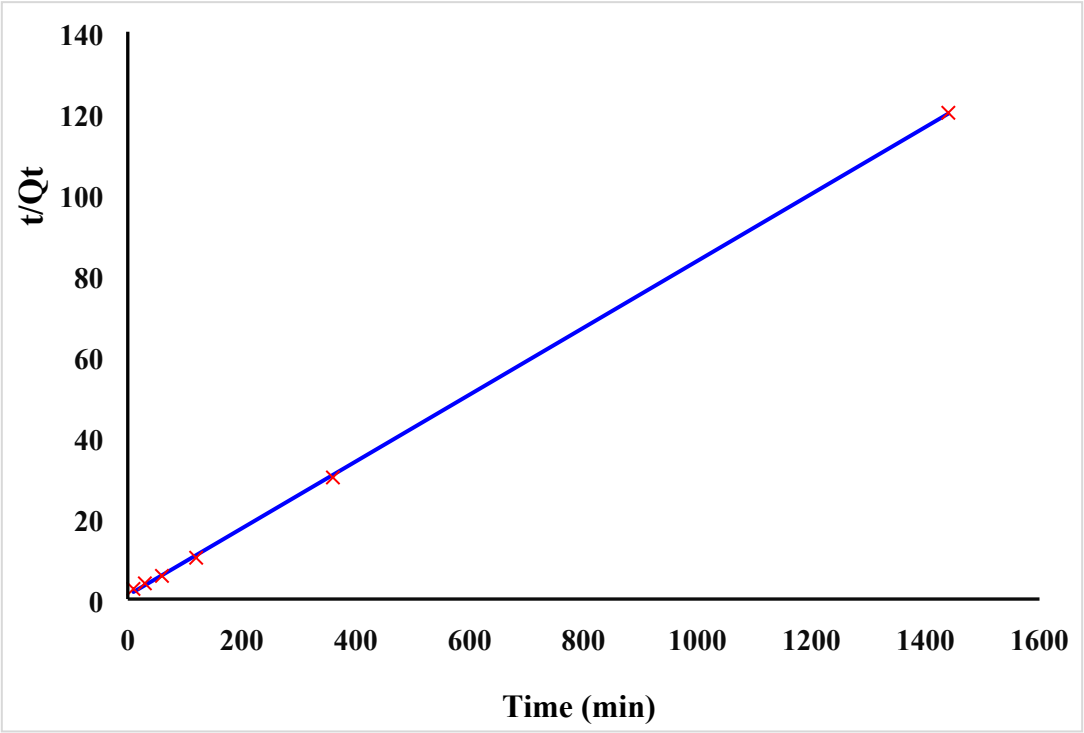

Fig. S13. Kinetic model of Pb(II) ions adsorption onto the COF@SO_3H adsorbent using pseudo-2nd-order.

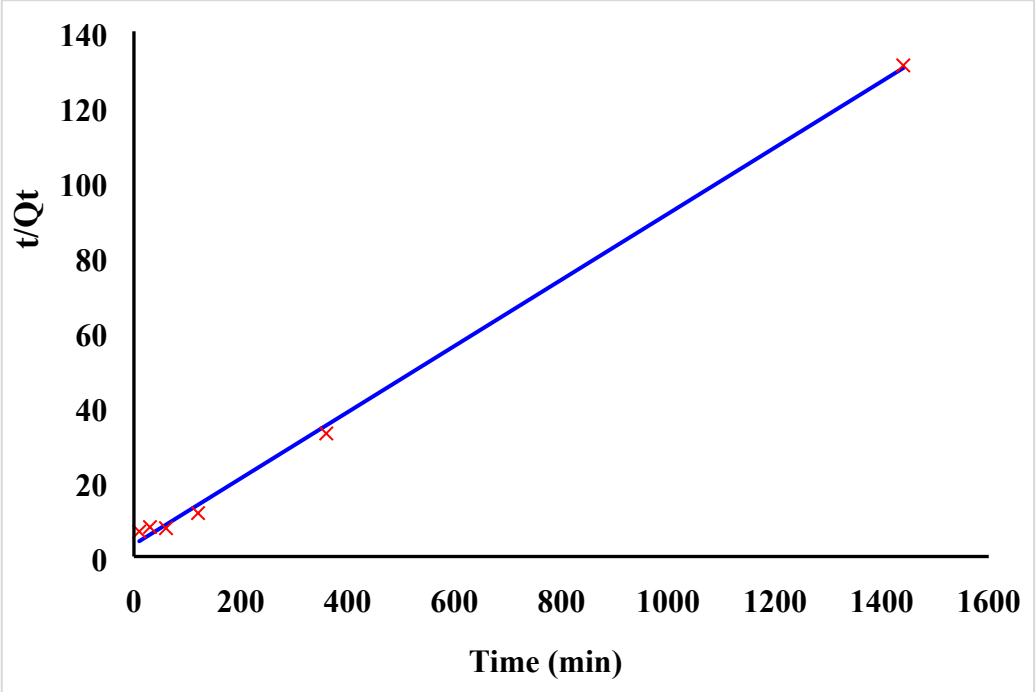

Fig. S14. Kinetic model of Ni(II) ions adsorption onto the COF@SO_3H adsorbent using pseudo-2nd-order.

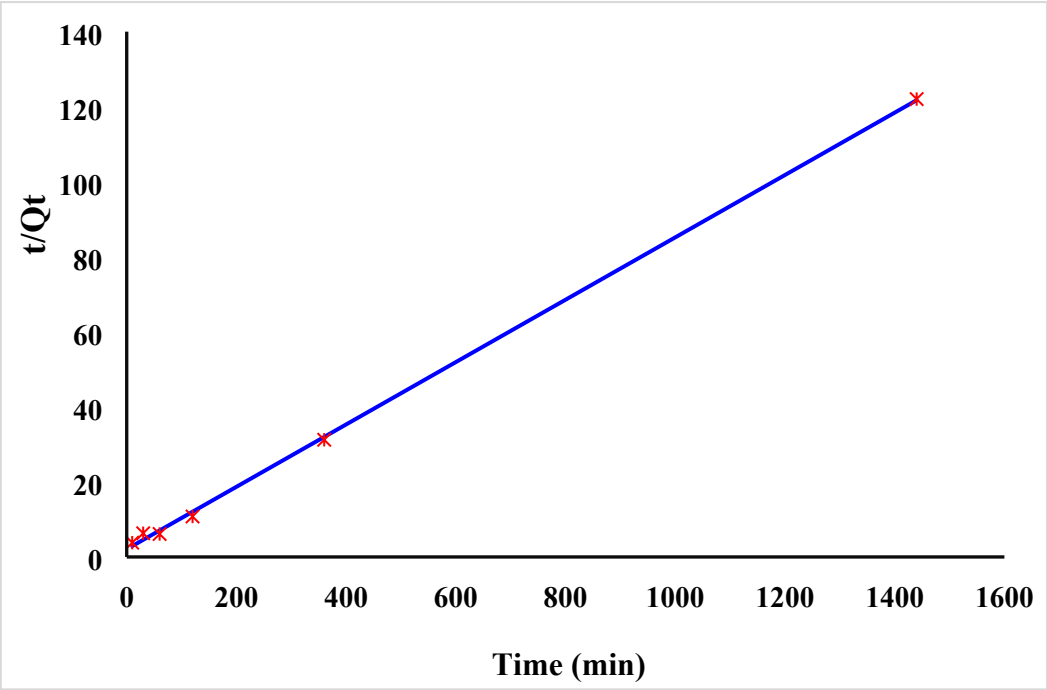

Fig. S15. Kinetic model of Zn(II) ions adsorption onto the COF@SO_3H adsorbent using pseudo-2^{nd}-order.

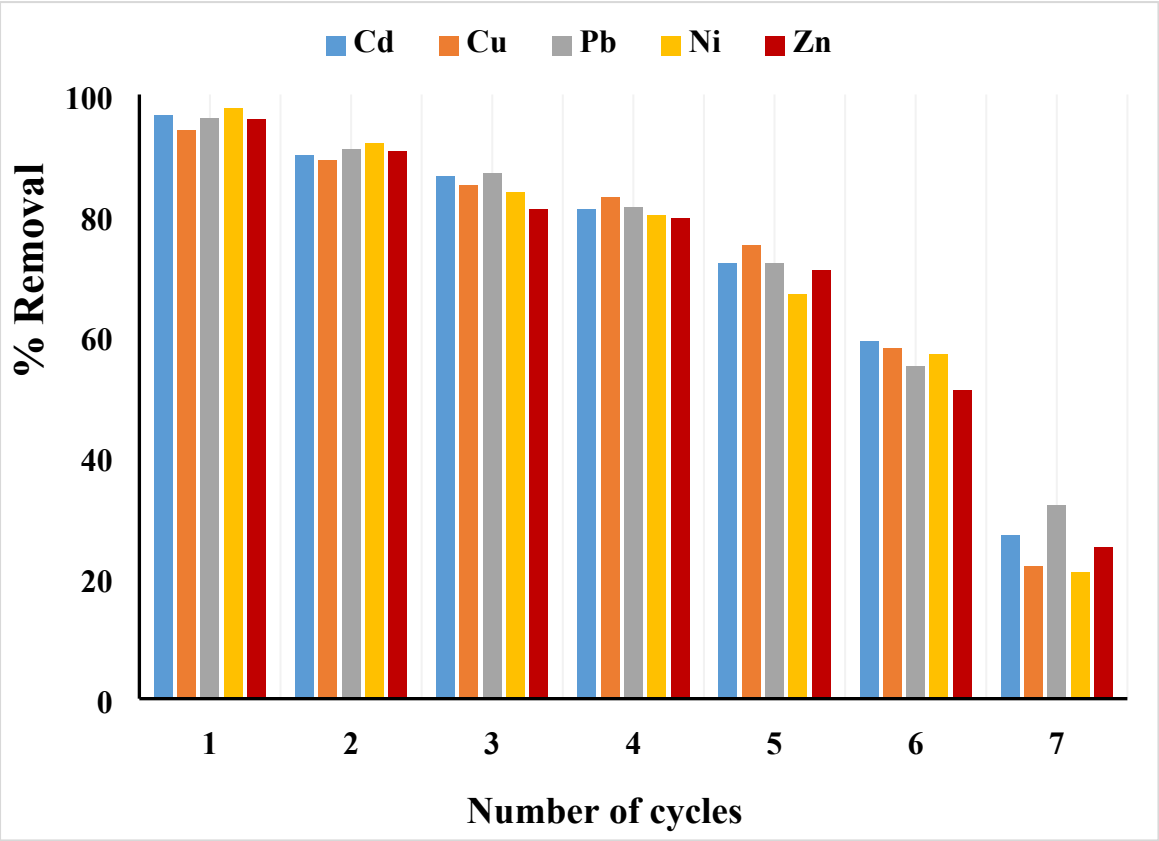

Fig. S16. Reusability study of COF@SO_3H adsorbent at different adsorption-desorption cycles.

1. Dehghani, M. H. *et al.* Statistical modelling of endocrine disrupting compounds adsorption onto activated carbon prepared from wood using CCD-RSM and DE hybrid evolutionary optimization framework: Comparison of linear vs non-linear isotherm and kinetic parameters. *Journal of Molecular Liquids* **302**, 112526, doi:https://doi.org/10.1016/j.molliq.2020.112526 (2020).
2. Bahrami, M., Amiri, M. J. & Bagheri, F. Optimization of the lead removal from aqueous solution using two starch based adsorbents: Design of experiments using response surface methodology (RSM). Journal of Environmental Chemical Engineering 7, 102793, doi:https://doi.org/10.1016/j.jece.2018.11.038 (2019).
3. Arabkhani, P., Javadian, H., Asfaram, A. & Hosseini, S. N. A reusable mesoporous adsorbent for efficient treatment of hazardous triphenylmethane dye wastewater: RSM-CCD optimization and rapid microwave-assisted regeneration. Scientific Reports 11, 22751, doi:10.1038/s41598-021-02213-2 (2021).
4. Hu, Q., & Zhang, Z. Application of Dubinin-Radushkevich isotherm model at the solid/solution interface: A theoretical analysis. Journal of Molecular Liquids, 277, 646-648. (2019).
5. Ayawei, N., Ebelegi, A.N. & Wankasi, D., 2017. Modelling and interpretation of adsorption isotherms. Journal of chemistry (2017).
6. Tamoradi Babaei, Z., Larki, A. & Ghanemi, K. Application of molybdenum disulfide nanosheets adsorbent for simultaneous preconcentration and determination of Cd(II), Pb(II), Zn(II) and Ni(II) in water samples. Journal of the Iranian Chemical Society, doi:10.1007/s13738-021-02289-7 (2021).
7. Javinezhad, S., Larki, A., Nikpour, Y. & Saghanezhad, S. J. Study on the Application of Cucurbit[6]uril as a Nanoporous Adsorbent for the Removal of 2,4-Dinitrophenol from Wastewaters Analytical and Bioanalytical Chemistry Research 5, 217-228, doi:10.22036/abcr.2018.113797.1180 (2018).
8. Hasani, N., Selimi, T., Mele, A., Thaçi, V., Halili, J., Berisha, A. &Sadiku, M. 2022. Theoretical, equilibrium, kinetics and thermodynamic investigations of methylene blue adsorption onto lignite coal. Molecules, 27(6), p.1856.